Int. J. Heat Mass Transfer. Vol. 25, No. 7, pp. 991–998, 1982
Printed in Great Britain

0017-9310/82/070991-08 $03.00/0
Pergamon Press Ltd.

HEAT TRANSFER BY STEADY LAMINAR FREE CONVECTION IN TRIANGULAR ENCLOSURES

V. A. AKINSETE
Mechanical Engineering Department, University of Lagos, Lagos, Nigeria

and

T. A. COLEMAN
Mechanical Engineering Department, University of Ilorin, Ilorin, Nigeria

(*Received* 17 *July* 1979 *and in final form* 10 *December* 1981)

Abstract—Two-dimensional laminar free convection in air contained in a long horizontal right-triangular enclosure has been investigated using numerical techniques. Steady-state solutions have been obtained for height–base ratios of $0.0625 \leqslant H/B \leqslant 1.0$ for Grashof number of $800 \leqslant Gr_{(B)} \leqslant 64\,000$. Results show that heat transfer across the base wall increases towards the hypotenuse/base intersection such that the third of the base length nearest the intersection accounts for about 60% of the heat transferred across the base. Results are well correlated by

$$\overline{Nu}_{(B)} = 1.102\,[Gr_{(B)}]^{0.0535}\,[H/B]^{-1.19}$$

for $0.0625 \leqslant H/B \leqslant 0.25$.

NOMENCLATURE

a, arbitrary constant;
B, base of triangular enclosure;
b, arbitrary constant;
c, arbitrary constant;
c_p, specific heat at constant pressure;
E_λ, neighbourhood length energy transport index;
f, general variable;
g, gravitational acceleration;
$Gr_{(B)}$, Grashof number, $g\beta B^3(T - T_{c,w})/\nu^2$;
$Gr^*_{(B)}$, modified Grashof number, $g\beta B^3(T_{h,w} - T_{c,w})/\nu^2$;
H, height of triangular enclosure;
k, thermal conductivity of fluid;
L, hypotenuse of triangular enclosure;
M, coordinate tangential to wall;
N, coordinate normal to wall;
$\overline{Nu}_{(B)}$, local Nusselt number for isothermal wall situation;
$Nu_{(B)}$, mean Nusselt Number for isothermal wall situation;
$Nu'_{(B)}$, local Nusselt number for constant heat flux situation;
$\overline{Nu}'_{(B)}$, mean Nusselt number for constant heat flux situation;
P, pressure;
Pr, Prandtl number, $\mu c_p/k$;
q, heat transfer rate;
$\bar{q}$, mean heat transfer rate;
q_w, local wall heat transfer rate;
T, temperature;
$T_{c,w}$, cold wall temperature;
$T_{h,w}$, hot wall temperature;
T_m, mean temperature;
u, velocity component in x-direction;
U, dimensionless velocity component in x-direction, uB/ν;
v, velocity component in y-direction;
V, dimensionless velocity component in y-direction, vB/ν;
w, subscript, for wall value;
x, independent coordinate in horizontal direction;
X, transformed x coordinate, x/B;
y, independent coordinate in vertical direction;
Y, transformed y coordinate, y/B.

Greek symbols

α, thermal diffusivity, $k/\rho c_p$;
β, fluid coefficient of cubical expansion;
ρ, fluid density;
γ, ratio q/k;
ψ, stream function;
Ψ, dimensionless stream function, ψ/ν;
Θ, dimensionless temperature, $(T - T_{c,w})/(T_{h,w} - T_{c,w})$; isothermal case;
Θ', dimensionless temperature, $(T - T_m)/(B\gamma)$; constant heat flux case;
ω, vorticity;
Ω, dimensionless vorticity, $B^2\omega/\nu$;
ν, kinematic viscosity of fluid;
μ, dynamic viscosity of fluid.

INTRODUCTION

THE PRESENT paper pertains to the natural convection flow in a right-triangular cavity with a horizontal base and heat input through the hypotenuse. The work has been motivated by the heat transfer problem associated with air-conditioning load calculations for pitched roofs with horizontal suspended ceiling. Also relevant is the heat transfer problem associated with roof-type solar stills and various other engineering structures. In spite of its obvious engineering importance, this problem has not been given the attention it deserves and air-conditioning calculations involving such configurations have had to be based on published data on pitched roofs with ceilings following the roof contours. The present work aims at obtaining the various heat and flow parameters for such enclosures as described above. Results are presented for the laminar-flow regime only with the added simplifications that the temperature of the heat source (the hypotenuse) is constant or that the heat input rate is constant. It has also been assumed that the cavity is isosceles-triangular in section so that the common boundary, the normal height of the section, can be taken as adiabatic. Perhaps the closest configuration to the present one is that of the rectangular cavity which has been studied by several authors. Theoretical investigations of laminar, natural convection in such enclosures have been undertaken by several authors including Batchelor [1], Elder [2], de Vahl Davis [3] and Newell and Schmidt [4] while results of experimental studies have been published by other investigators such as Elder [5] and Yin *et al.* [6]. Pnueli [7] examined the thermal instability in confined fluids in cylindrical enclosures while Hollands [8] investigated that in rectangular enclosures with honeycomb constraint. Comprehensive reviews of various works on natural convection in closed cavities have been published by Ostroumov [9], Eckert and Carlson [10] and Wilkes [11]. In view of the differences in geometry of the enclosures and the methods of heat input, the results of the above authors do not lend themselves to easy interpretation of the processes involved in the present problem.

Physical model

Before obtaining solutions to the various conservation equations associated with the problem, it is essential to define a physical model of the problem. Such a model will usually be different from the real problem, but the differences should be such as not to mask the important physical processes associated with the problem.

The model adopted for the present work is that of a 2-dim. enclosure with a right triangular cross-section (Fig. 1). Fluid motion is set up by heating the hypotenuse which may be deemed as representing the pitched roof while cooling the horizontal base which in turn represents the suspended ceiling. The third side, the vertical height, is assumed to be adiabatic and hence can be said to represent the boundary between the two identical halves of the isosceles triangular cavity. Two situations are considered depending on the conditions stipulated at the hot wall (the hypotenuse). These are

Case I. The hot wall is isothermal.

Case II. There is constant heat flux through the hot wall.

For Case (I), the cold wall (the horizontal base) is assumed to be isothermal, while for Case (II), constant rate of cooling is assumed on this wall.

ASSUMPTIONS AND GOVERNING EQUATIONS

The assumptions made for the ensuing analysis are as follows:

(1) The flow is laminar and 2-dim.
(2) Viscous dissipation can be neglected.
(3) No internal heat source or sink is involved.
(4) The fluid is Newtonian.
(5) Fluid properties are constant except in the formulation of the buoyancy term.
(6) Compressibility effects are negligible.

From Fig. 1 and by invoking the above assumptions, the basic conservation laws of mass, momentum and energy can be written in the following dimensionless forms:

Temperature field equation

$$\frac{\partial^2\Theta}{\partial X^2} + \frac{\partial^2\Theta}{\partial Y^2} = Pr\left[U\frac{\partial\Theta}{\partial X} + V\frac{\partial\Theta}{\partial Y}\right] \tag{1}$$

Vorticity field equation

$$\frac{\partial^2\Omega}{\partial X^2} + \frac{\partial^2\Omega}{\partial Y^2} = U\frac{\partial\Omega}{\partial X} + V\frac{\partial\Omega}{\partial Y} - Gr_{(B)}\frac{\partial\Theta}{\partial X} \tag{2}$$

Stream function field equation

$$\frac{\partial^2\Psi}{\partial X^2} + \frac{\partial^2\Psi}{\partial Y^2} = -\Omega \tag{3}$$

Velocity field equations

$$U = \frac{\partial\Psi}{\partial Y} \tag{4}$$

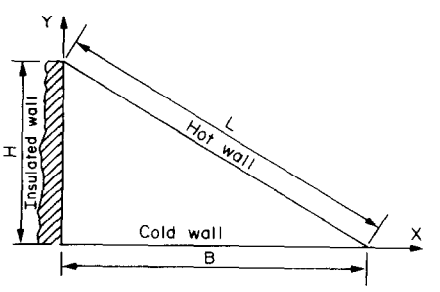

FIG. 1. Physical model.

and

$$V = -\frac{\partial \Psi}{\partial X} \tag{5}$$

Boundary conditions

Velocities. On all the walls

$$U_w = V_w = 0. \tag{6}$$

Temperature. On the adiabatic wall

$$\left.\frac{\partial \theta}{\partial X}\right|_{X=0} = 0 \tag{7}$$

On the horizontal wall,

Case (I) (Isothermal)

$$\theta_{c,w} = 0 \tag{8}$$

Case (II) (Constant heat flux):

$$\left.\frac{\partial \theta}{\partial X}\right|_{Y=0} = \text{constant} \tag{9}$$

On the inclined wall,

Case (I) (Isothermal):

$$\Theta_{h,w} = 1 \tag{10}$$

Case (II) (Constant heat flux):

$$\frac{\partial \Theta}{\partial N} = \text{constant} \tag{11}$$

Stream function. From equations (4)–(6)

$$\left.\frac{\partial \Psi}{\partial N}\right|_w = \left.\frac{\partial \Psi}{\partial M}\right|_w = 0. \tag{12}$$

It follows that Ψ_w is constant on all walls. Without any loss of generality, Ψ_w is set to zero

$$\text{i.e.} \quad \Psi_w = 0 \tag{13}$$

Vorticity. No explicit boundary conditions can be specified for Ω. However, at any step in the iterative process employed in solving the system of equations, values of U and V obtained from the solution of equations (4) and (5) are used to estimate Ω from the equation relating vorticity and velocity derivatives. In dimensionless form, this equation becomes

$$\Omega = \frac{\partial V}{\partial X} - \frac{\partial U}{\partial Y}. \tag{14}$$

This method has been employed by Aziz and Hellums [12] and Newell and Schmidt [4]. The latter authors reported that the use of this method results in relatively small truncation errors while yielding reasonably stable results.

Finite-difference representations of the differential equations

In order to obtain solutions to the system of equations by numerical methods, each of the governing differential equations is replaced with its finite difference representation. To achieve this, the entire triangular region is divided into a mesh system with equal numbers of divisions in the X and Y directions. This ensures that the hypotenuse lies on grid intersections. The finite difference representation is then applied to the nodes of the mesh system.

Central difference representations are used for equations (1)–(3), yielding three sets of implicit non-linear simultaneous difference equations. In addition, the replacement of equations (4) and (5) with central difference representations results in two sets of explicit equations. The five equations have to be satisfied simultaneously by the required solutions.

Representations for regions adjacent to the walls where the condition $\partial f/\partial N = 0$ holds are separately developed using a method outlined by Newell and Schmidt [4]. The representation for the estimates of boundary vorticity was similarly treated. Considering the inclined wall as an 'irregular' boundary, representations for these conditions at this wall are developed by making use of direction cosines and approximations for normal derivatives on this boundary.

Nusselt numbers

The energy transported across the horizontal wall is expressed in terms of local and mean Nusselt numbers. The Nusselt numbers defined for the horizontal wall are

Case I (Isothermal):

Local Nusselt Number,

$$Nu_{(B)} = \left.\frac{\partial \theta}{\partial Y}\right|_{Y=0} \tag{15}$$

Mean Nusselt Number,

$$\overline{Nu}_{(B)} = \frac{1}{B}\int_0^B \left.\frac{\partial \theta}{\partial Y}\right|_{Y=0} \mathrm{d}x \tag{16}$$

Case (II) (Constant heat flux)

Local Nusselt Number,

$$Nu'_{(B)} = \left[\frac{1}{\theta_{c,w}}\right]\left.\frac{\partial \theta}{\partial Y}\right|_{Y=0} \tag{17}$$

Mean Nusselt Number,

$$\overline{Nu}'_{(B)} = \frac{1}{B}\int_0^B Nu'_{(B)}\,\mathrm{d}X \tag{18}$$

The integrations in equations (16) and (18) were performed using the Trapezoidal Rule.

Method of solution of difference equations

The finite difference representations of normalized equations (1)–(3) were solved by an iterative scheme following a cyclical sequence. First, the representation of equation (1) was solved for θ, treating U and V as known functions. Initially, test values ($U = 0$ and $V = 0$) were assigned and the iteration carried out until the solution converged subject to the satisfaction of a convergence criterion.

The second stage involved the solution of equation (2) for Ω, using the values of θ obtained in the first stage and the initial values of U and V. Initially, an arbitrary boundary distribution was used for Ω. This arbitrary distribution was replaced in the next cycle of iteration by estimates of Ω obtained by using the estimates of U and V from equation (14). The third stage in the iteration involved the solution of the representation of equation (3) for Ψ using the values of Ω obtained from the previous stage. The method of iteration here was similar to those of the first two stages, the boundary condition used being $\Psi = 0$.

The explicit representations of equations (4) and (5) were finally solved for U and V, using the most recently obtained Ψ distribution.

This completed the first phase of the iterative operation. Next, the values obtained in the first operation were used to repeat the entire operation for the second cycle thus obtaining new distributions for θ, Ω, Ψ etc. The operation was repeated until the desired accuracy was achieved. This accuracy was assessed in terms of the invariability of each field at the end of two successive cycles. For practical purposes, each field was considered invariable if the absolute values of the difference between field values for two successive cycles were less than 10^{-4}.

The above calculations were carried out for each of the two cases described above.

A Gauss–Seidel iteration routine was used to solve the sets of implicit equations and a WATFIV computer program was written to execute all the required calculations.

For each set of cavity ratio and Grashof number, calculations were carried out with the triangular region divided into a grid system having equal increments in both the X and Y directions. Initially, computations were carried out for ten equal increments in both the X and Y directions (11 × 11 mesh). Subsequently, in order to investigate the validity of the solutions, as well as to examine the effect of changing mesh sizes, the calculations were repeated for a 17 × 17 mesh i.e. sixteen equal increments in both the X and Y directions. Results in this work have been presented from the 17 × 17 mesh.

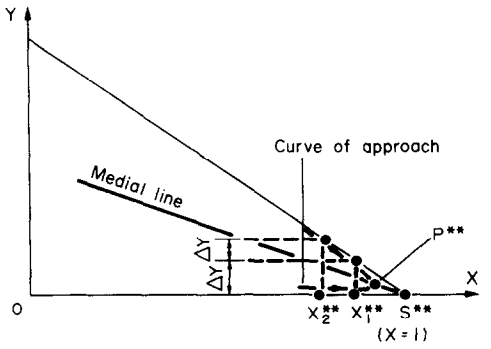

FIG. 2. Conditions near point of singularity.

Point of singularity, X = 1

It will be seen that the point of intersection of the hot and cold walls of the triangular enclosure is a point of singularity introduced by having different temperatures on the two intersecting walls. The conditions in the neighbourhood of this singularity are illustrated in Fig. 2. As this point is approached, the difference representation of the derivative $(\partial\theta/\partial Y)|_{Y=0}$ used for evaluating the Nusselt numbers in equations (15)–(18) no longer applies near the boundary since there are no mesh points near this wall and close to the singularity. The use of this representation does not therefore permit the limiting value of the Nusselt number to be determined as the singularity is approached.

The method used in the present study to determine the limiting value of $Nu_{(B)}$ is similar to that outlined by Collatz [14]. By this method, the singularity S^{**} (Fig. 2) is approached from the hot and cold walls simultaneously along the curve of approach represented by a parabolic profile described by a temperature relation of the form

$$\Theta = AY^2 + BY + C \tag{19}$$

and passing through the three wall nodes closest to the singularity. The constants A, B and C in equation (19) are determined by using the values of $\theta(\theta_{c1}^{**}, \theta_{h1}^{**}$ and $\theta_{h2}^{**})$ and the corresponding mesh values of $Y(0, \Delta Y$, and $2\Delta Y$ respectively, where ΔY is the mesh spacing in the Y-direction) at the three nodes.

The next step is to solve for a parabolic spatial relation of the form

$$X = DY^2 + EY + G \tag{20}$$

which also describes the curve, and finding the constants D, E and G by using the three values of $X(X_1^{**}$, X_1^{**} and $X_2^{**})$ at the three wall nodes close to the singularity along with their corresponding Y values (0, ΔY and $2\Delta Y$ respectively).

A medial line is now projected from the singularity to intersect the curve at a point P^{**} very close to the singularity and tending to coincide with it as the mesh divisions become progressively smaller. The value of $Nu_{(B)}$ at P^{**} is taken to be the required limiting value corresponding to the singularity for any given mesh system. The medial line can be represented by an equation of the form

$$X = QY + R \tag{21}$$

where Q and R are constants determined by using the conditions that $Y = 0$ when $X = B$, and $X = 0$ when $Y = H/2$ (B and H represent the base and the height if the cavity respectively). The line and curve make an intercept at the position P^{**} at which the value of Y makes equations (20) and (21) identical. If this value of Y is Y^{**}, then the required limiting value of $Nu_{(B)}$ is obtained by taking the derivative $(\partial\theta/\partial Y)$ of equation (19) and substituting Y^{**} into the result of the differentiation.

The resulting relation is of the form

$$Nu^{**}_{(B)} = \left.\frac{\partial\theta}{\partial Y}\right|_{Y^{**}} = \delta Y^{**} + \varepsilon \qquad (22)$$

where δ and ε involve the quantities $\theta^{**}_{h_1}$, $\theta^{**}_{h_2}$, $\theta^{**}_{c_1}$, and ΔY, while Y^{**} is the quadratic root involving ΔY, X^{**}_1, X^{**}_2, B and H and having a value less than ΔY.

DISCUSSION

The results presented are for $Pr = 0.733$ and for $Gr_{(B)}$ covering the range 800–64 000. The ratios of height–base considered are $0.0625 \leq H/B \leq 1$. The mesh system constructed for finite difference discretization consisted of mesh lines that made grid intersections on the hypotenuse of the triangular region. Equal intervals along the X and Y axes were used for all the ratios considered. This further implied that the total numbers of divisions along the X-axis, Y-axis and the inclined wall were always equal for any number of mesh divisions. Finally, the system employed made the ratio $\Delta Y/\Delta X$ equal to H/B for all cases which considerably simplified computational problems. Results obtained for the two cases of isothermal hot hypotenuse and cold base [Case (I)] and constant heat input rates on the hypotenuse [Case (II)] show close similarities in many aspects.

An indication of heat transported across the horizontal base wall of the triangular region is shown in Fig. 3. The local Nusselt number $Nu_{(B)}$ increases to a definite value at the intersection between the base wall and the inclined wall.

The high values of $Nu_{(B)}$ near the intersection give an indication that a given region within the neighbourhood of this intersection accounts for more than a proportionate amount of heat transported across the base wall. This indication is supported by reference to Fig. 4 which shows the percentage heat transport for a neighborhood length λ, defined as the third of the length of the base wall nearest the intersection. For this length, a neighborhood energy transport index, E_λ, is defined, and is computed by integrating the local Nusselt numbers over λ and expressing this integral as a percentage of the integral of $Nu_{(B)}$ over the entire base wall. It is seen that for the cases of H/B ratios considered this neighborhood length accounts for more than 60% of the heat transported across the base wall.

The practical significance of this result is that the heat transported across the base can be most effectively extracted by placing a heat extraction device at a position very close to the region specified by λ. The comparative curve shown for the constant heat flux case in Fig. 4 shows only a slight drop in E_λ.

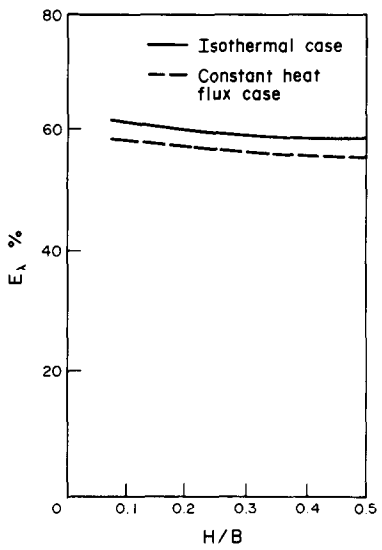

FIG. 4. Neighborhood length energy transport index vs H/B.

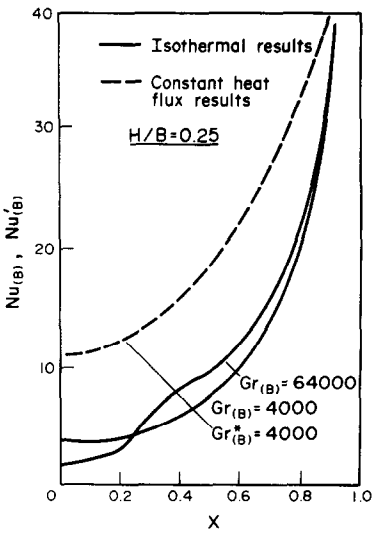

FIG. 3. Local Nusselt number vs X.

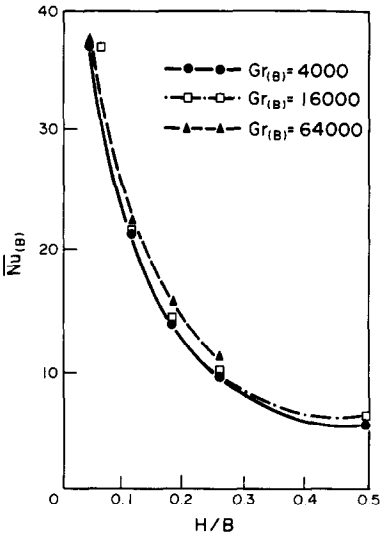

FIG. 5. Mean Nusselt number vs H/B for isothermal hot wall.

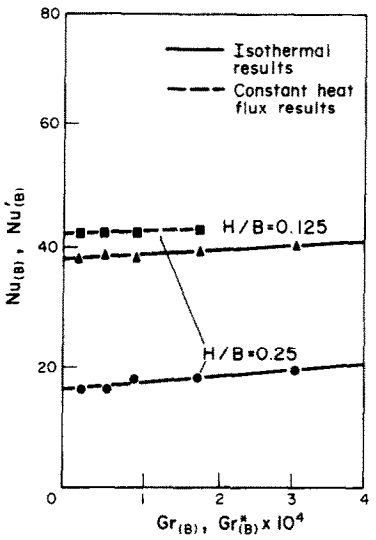

FIG. 6. Mean Nusselt number vs Grashof number.

An example of the variation of the mean Nusselt number $\overline{Nu}_{(B)}$ with H/B is shown in Fig. 5. For a given Grashof number, increasing the height/base ratio gives rise to sharp drops in the amount of heat transported across the base wall. This result is to be expected because most of the heat transfer across the base wall occurs near the intersection between the base and the hypotenuse: hence increasing the height of the region does little to increase the total heat transferred. It follows that in practice, for a given Grashof number (characterising the thermal condition imposed on the hot wall), the higher the H/B ratio, the less the heat transferred across the base wall.

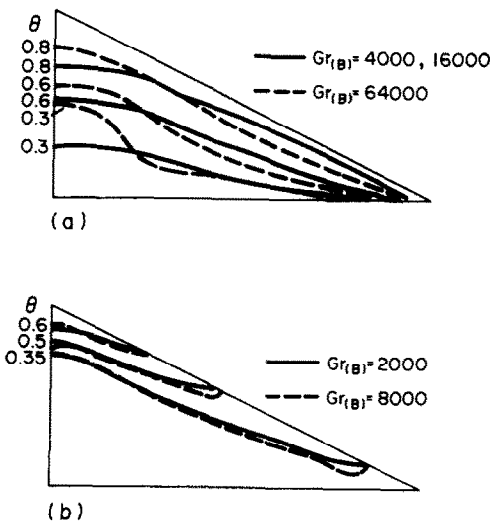

FIG. 7(a). Isotherms for $H/B = 0.25$ for isothermal case. (b). Isotherms for $H/B = 0.25$ for constant heat flux case.

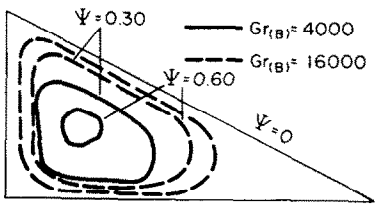

FIG. 8. Streamlines for $H/B = 0.25$.

The variation of the mean Nusselt number $\overline{Nu}_{(B)}$ with $Gr_{(B)}$ is shown in Fig. 6. $\overline{Nu}_{(B)}$ changes very slightly with $Gr_{(B)}$ over most of the ranges of Grashof numbers considered. It is observed that these changes are more pronounced for higher H/B ratios than for lower ratios.

The effect of $Gr_{(B)}$ on the steady state dimensionless temperature distribution θ is shown in Fig. 7(a). Isotherm maps for the entire triangular region for which $H/B = 0.25$ are displayed for three values of $Gr_{(B)}$. The isotherms emerge normally from the adiabatic wall and converge towards the intersection of the hypotenuse and the base wall. At a relatively low $Gr_{(B)}$ of about 4000, the effect of convection on the isotherms is minimal. When $Gr_{(B)}$ is increased to about 16 000, the change in the isotherms is hardly noticeable. This situation is similar to that of pure conduction. Noticeable changes in the isotherms begin to take place only for relatively high values of Grashof number. As an example, for $Gr_{(B)}$ of 64 000, the effect of the adiabatic wall extends into the region of the enclosure near the central section. The isotherms are pushed towards the hot wall for approximately the first quarter of the width of the enclosure nearest the adiabatic wall. For the remaining distance, the isotherms are pushed downward towards the cold wall. This pattern of the temperature field bears some similarity to two boundary layer formations, one growing downward along the hot wall, and the other growing upward towards the insulated wall along the base wall. The sudden depression of the near-middle sections of the isotherms indicates the possibility of separation occurring in the primary flow around these sections. Figure 7(b) shows corresponding isotherm maps for the constant heat flux situation [Case (II)]. Here, isotherms leave as normals to the adiabatic wall and end up on the inclined wall. An indication of the sensitivity of the stream lines to changes in the Grashof number is shown in Fig. 8. Stream-lines of specified strength tend to recede towards the walls of the enclosure as $Gr_{(B)}$ is raised. It is observed that stream-lines of relatively greater strengths are centred around that portion of the enclosure where the sudden depressions of isotherms occur.

In order to obtain a correlation between $Nu_{(B)}$, $Gr_{(B)}$ and H/B, sets of 3-dim., linear, logarithmic simultaneous equations were solved by making use of Fig. 5 for an expression of the form

$$\overline{Nu}_{(B)} = c[Gr_{(B)}]^a [H/B]^b.$$

The above form was obtained from a dimensional analysis using the concepts of Vector Lengths. The resulting expression is

$$\overline{Nu}_{(B)} = 1.102\,[Gr_{(B)}]^{0.535}\,[H/B]^{-1.19}$$

This correlation holds reasonably well for H/B ratios of $0.0625 \leq H/B \leq 0.25$ and Grashof numbers over the range $4000 \leq Gr_{(B)} \leq 64\,000$. This result shows the high influence of the parameter H/B and the lesser influence of $Gr_{(B)}$ on $\overline{Nu}_{(B)}$ for equivalent changes in the two parameters, a deduction which has already been mentioned from other observations.

For a proper evaluation of the results presented, an investigation was made of the effect of changing grid sizes on the numerical solutions. Newell and Schmidt [4] and Azis and Hellums [12] have noted that refinement of grid sizes tends to cause changes in the Nusselt number. For example, in going from 11 × 11 mesh to 41 × 41 mesh, Azis and Hellums reported a change of 40% in the Nusselt number.

The present work tends to agree with the assertion of Newell and Schmidt that, among other things, the mesh size and the order of the finite difference approximation significantly influence the accuracy of the Nusselt numbers. In this work, it was observed that in going from 11 × 11 mesh to 17 × 17 mesh there was an increase of about 11% in the value of the Nusselt number. The refinement of grid sizes also tended to increase the number of iterations required to achieve convergence for each field.

CONCLUSIONS

Analysis has been carried out for heat transfer by steady, laminar, free convection in a triangular enclosure. It has been found that a considerable proportion of the heat transfer across the base wall of the region takes place near the intersection of the base and the hypotenuse. The relationship between the mean Nusselt number, $\overline{Nu}_{(B)}$, the Grashof number, $Gr_{(B)}$, and the height–base ratio, H/B, is such that for equivalent changes in $Gr_{(B)}$ and H/B, the influence of H/B is the considerably higher factor. The two cases examined, namely isothermal hot wall and constant heat flux situations, show close similarities in several respects.

REFERENCES

1. G. K. Batchelor, Heat transfer by free convection across a closed cavity between vertical boundaries at different temperatures, *Q. Appl. Math* **12**, 209–233 (1954).
2. J. W. Elder, Numerical experiments with free convection in a vertical slot, *J. Fluid Mech.* **24**, 823–843 (1966).
3. G. De Vahl Davis, Laminar natural convection in an enclosed rectangular cavity, *Int. J. Heat Mass Transfer* **11**, 1675–1693 (1968).
4. M. E. Newell, and F. W. Schmidt, Heat transfer by laminar natural convection within rectangular enclosures, *Am. Soc. Mech. Engrs*, Series C, *J. Heat Transfer* **XX**, 159–168 (1970).
5. J. W. Elder, Laminar free convection in a vertical slot, *J. Fluid Mech.* **23**, 77–98 (1965).
6. S. H. Yin, T. Y. Wung, and K. Chen, Natural convection in an air layer enclosed within rectangular cavities, *Int. J. Heat Mass Transfer* **21**, 307–315 (1978).
7. D. Pnueli, The thermal instability of confined fluids, Ph.D. Thesis, Case Institute of Technology (1962).
8. K. G. T. Hollands, Natural Convection in a horizontal layer of air with internal constraints, Ph.D. Thesis, McGill University (1966).
9. G. A. Ostroumov, Free convection in closed cavities. A review of work carried out at Perm, USSR, *Int. J. Heat Mass Transfer* **8**, 259–268 (1964).
10. E. G. R. Eckert, and W. O. Carlson, Natural convection in an air layer enclosed between two vertical plates with different temperatures, *Int. J. Heat Mass Transfer* **2**, 106–121 (1961).
11. J. O. Wilkes, The finite difference computation of natural convection in an enclosed rectangular region, Ph.D. Thesis, University of Michigan (1963).
12. K. Aziz and J. D. Hellums, Numerical solution of the three dimensional equations of motion for laminar natural convection, *Physics Fluids* **10**, 314–324 (1967).
13. J. O. Wilkes and S. O. Churchill, The finite difference computation of natural convection in a rectangular enclosure, *A.I.Ch.E.Jl* **12**, 161–166 (1966).
14. L. Collatz, *The numerical treatment of differential equations*. Springer, Berlin (1966).

TRANSFERT THERMIQUE PAR CONVECTION NATURELLE PERMANENTE DANS DES ENCEINTES TRIANGULAIRES

Résumé—On étudie par voie numérique la convection naturelle bidimensionnelle, laminaire dans l'air contenu dans une enceinte longue, horizontale à section droite en triangle rectangle. Des solutions permanentes sont obtenues pour des rapports hauteur sur base $0{,}0625 \leqslant H/B \leqslant 1{,}0$ et pour un nombre de Grashof $800 \leqslant Gr_{(B)} \leqslant 64\,000$. Les résultats montrent que le transfert thermique à travers la base augmente vers l'arête commune à l'hypoténuse et la base, si bien que le tiers de la base vers cette arête compte pour 60% de la chaleur totale transférée. Les résultats sont bien représentés par:

$$\overline{Nu}_{(B)} = 1{,}102\,[Gr_{(B)}]^{0{,}0535}\,[H/B]^{-1{,}19}$$

pour $0{,}0625 \leqslant H/B \leqslant 0{,}25$.

WÄRMETRANSPORT BEI STATIONÄRER LAMINARER FREIER KONVEKTION IN DREIECKIGEN HOHLRÄUMEN

Zusammenfassung—Es wurde zweidimensionale laminare freie Konvektion in Luft numerisch untersucht, die in einem langen, horizontalen, rechtwinklig-dreieckigen Hohlraum eingeschlossen ist. Lösungen für den stationären Zustand wurden für Verhältnisse von Höhe zu Grundseite im Bereich von $0{,}0625 \leqslant H/B \leqslant 1{,}0$ und Grashof-Zahlen im Bereich von $800 \leqslant Gr_{(B)} \leqslant 64\,000$ erhalten. Die Ergebnisse zeigen eine Zunahme des Wärmetransports durch die Wand der Grundseite zum Schnittpunkt von Hypotenuse und Grundseite hin, so daß das dem Schnittpunkt nächstliegende Drittel der Grundseitenlänge mit 60% zu der an der Grundseite übertragenen Wärme beiträgt. Für den Bereich von $0{,}0625 \leqslant H/B \leqslant 0{,}25$ werden die Ergebnisse gut korreliert durch die Gleichung

$$\overline{Nu}_{(B)} = 1{,}102\,[Gr_{(B)}]^{0.0535}\,[H/B]^{-1.19}.$$

ТЕПЛОПЕРЕНОС ПРИ СТАЦИОНАРНОЙ ЛАМИНАРНОЙ СВОБОДНОЙ КОНВЕКЦИИ В ТРЕУГОЛЬНЫХ ПОЛОСТЯХ

Аннотация — Численными методами исследуется двумерная ламинарная свободная конвекция в содержащей воздух длинной горизонтальной полости, имеющей сечение в форме прямоугольного треугольника. Получены стационарные решения для отношений высоты треугольника к основанию в диапазоне $0{,}0625 \leq H/B \leq 1{,}0$ при значениях числа Грасгофа $800 \leq Gr_{(B)} \leq 64\,000$. Результаты показывают, что плотность теплового потока через основание возрастает по направлению к месту пересечения гипотенузы с основанием, так что через треть длины основания, расположенной возле пересечения, проходит примерно 60% тепла, переносимого через все основание. Результаты хорошо описываются соотношением

$$\overline{Nu}_{(B)} = 1{,}102[Gr_{(B)}]^{0.0535}[H/B]^{-1.19}$$

при $0{,}0625 \leq H/B \leq 0{,}25$.